Chemical Science

EDGE ARTICLE

View Article Online
View Journal | View Issue

Cite this: *Chem. Sci.*, 2016, 7, 5441

Dendronized delayed fluorescence emitters for non-doped, solution-processed organic light-emitting diodes with high efficiency and low efficiency roll-off simultaneously: two parallel emissive channels†

Yifan Li,‡ Guohua Xie,‡ Shaolong Gong, Kailong Wu and Chuluo Yang*

Received 29th February 2016
Accepted 23rd April 2016

DOI: 10.1039/c6sc00943c

www.rsc.org/chemicalscience

We have developed two new carbazole-dendronized emitters based on a green emissive thermally activated delayed fluorescence (TADF) core. Both dendrimers possess excellent thermal stability, good solution processability, and an obvious TADF feature. Non-doped OLEDs based on the emitters formed by a solution process exhibit a maximum external quantum efficiency (EQE) of 13.8%. Remarkably, the EQE remains as high as 13.3% at the high luminance of 1000 cd m^{-2}. To the best of our knowledge, this is one of the highest EQE values for dendrimer-based fluorescent OLEDs, which nearly harvest all of the generated excitons and exhibit a considerably low loss of EQE estimated from 1000 to 5000 cd m^{-2}. Furthermore, we reveal a new emissive approach to utilize the excitons by a combination of both TADF and exciplex emission.

Introduction

Metal-free thermally activated delayed fluorescence (TADF) emitters have recently aroused considerable attention because they can harvest both singlet and triplet excitons through up-converting non-radiative triplet excitons to radiative singlet excitons and thereby approach a theoretical internal quantum efficiency (IQE) of 100%.[1,2] Highly efficient OLEDs based on TADF emitters have achieved maximum external quantum efficiencies (EQEs) over 20%, which are comparable with heavy-metal based phosphorescent OLEDs. For example, the devices based on a blue emitter of a triazine/carbazole hybrid, and a green emitter of 2,4,5,6-tetra(carbazol-9-yl)-1,3-dicyanobenzene (4CzIPN) have achieved EQEs of 20.6% and 28.6%, respectively.[1b,2b,3] In addition to the TADF emitters, the exciplex emission formed between electron-donating and electron-accepting molecules has recently been demonstrated to be promising for highly efficient fluorescent OLEDs.[4] For example, the highest EQE of 15.4% for a fluorescent OLED employing an exciplex with a high photoluminescence quantum yield (PLQY) of 0.68 has been reported.[5]

Despite the high efficiency of these two types of emissive approaches in fluorescent OLEDs, further utilization of these emitters in the solution process has been rarely explored.[6] Generally, most highly efficient devices are fabricated *via* vacuum evaporation technology, which requires a complicated process, high costs and precise engineering. Comparatively, solution processes, such as spin-coating and ink-jet printing, represent low-cost methods to fabricate large-area OLEDs.[7] In the past three years, OLEDs based on solution-processable TADF emitters have made some progress. For example, Lee *et al.* reported a solution-processed OLED with a maximum EQE of 18.3% by utilizing a green TADF emitter;[8] Su *et al.* demonstrated a maximum EQE of 17.5% by employing an evaporation- and solution-process-feasible TADF emitter.[9] Although these devices exhibited good performance, all of the emitting layers (EMLs) in the devices are host:dopant systems that require precise control and may result in phase separation. In these contexts, developing solution-processed non-doped emissive materials with a TADF feature is of practical and important significance.

Carbazole-dendronized materials are promising single-component functional materials for solution-processed OLEDs because of their good solubility in common solvents, good hole-transporting ability, amorphous film-forming property, and high thermal stability.[10]

Although some progress has been made on carbazole-dendronized phosphorescent emitters,[11] much work remains to be done with the aim of developing metal-free emitters with

Hubei Collaborative Innovation Center for Advanced Organic Chemical Materials, Hubei Key Lab on Organic and Polymeric Optoelectronic Materials, Department of Chemistry, Wuhan University, Wuhan, 430072, People's Republic of China. E-mail: clyang@whu.edu.cn

† Electronic supplementary information (ESI) available: Thermal, photophysical, and electrochemical data of the materials, TGA curves, DSC curves, CV curves, AFM topographic images, DFT calculation, EL spectra of Devices A1–C4, various current densities and efficiency *versus* luminance curves for Devices A1–C4 and ^{1}H NMR spectrum. See DOI: 10.1039/c6sc00943c

‡ These authors contributed equally to this work.

a high EQE for solution-processed OLEDs. In this communication, we report two carbazole-dendronized TADF emitters by introducing carbazole dendrons into a TADF emissive core, bis(4-(9,9-dimethylacridin-10(9*H*)-yl)phenyl)methanone (**DMAC-BP**), which has been proven to be an excellent green TADF emitter peaking at 506 nm in neat film with a high PLQY of 0.85.[12] We anticipate that the decoration of **DMAC-BP** with carbazole could not only improve hole injection and transport ability, but also minimize the exciton quenching approach, and consequently reduce efficiency roll-off at high luminance. Double-layer devices based on these emitters as the non-doped emissive layer exhibit a maximum EQE of 13.8%. Remarkably, the EQE remains at 13.3% at the high luminance of 1000 cd m^{-2}. To the best of our knowledge, this is one of the highest EQE values for dendrimer-based fluorescent OLEDs. Furthermore, we reveal that the dendrimer-based devices display a dual-channel emissive feature, *i.e.*, both TADF and interfacial exciplex emission.

Results and discussion

The chemical structures of two carbazole-dendronized emitters, named bis(4-(2,7-bis(3,6-di-*tert*-butyl-9*H*-carbazol-9-yl)-9,9-dimethylacridin-10(9*H*)-yl)phenyl)methanone (**CDE1**) and bis(4-(2,7-bis(3,3″,6,6″-tetra-*tert*-butyl-9′*H*-[9,3″:6′,9″-tercarbazole]-9″-yl)-9,9-dimethylacridin-10(9*H*)-yl)phenyl)methanone (**CDE2**), are depicted in Fig. 1. Iodization of **DMAC-BP** with *N*-iodosuccinimide (NIS) produced the key intermediate, bis(4-(2,7-diiodo-9,9-dimethylacridin-10(9*H*)-yl)phenyl)methanone (4IDMACBP),[13] which was coupled with the first and second generation carbazole dendrons through the Ullmann C–N coupling reaction to afford the target compounds **CDE1** and **CDE2**, respectively (Scheme S1†).[6a] These compounds were characterized by ^{1}H NMR and ^{13}C NMR spectroscopies, mass spectrometry, and elemental analysis. The two compounds exhibit superior solubility in usual organic solvents, such as dichloromethane, tetrahydrofuran, toluene, and chlorobenzene, due to the peripheral *tert*-butyl groups. Their good thermal stability was indicated by the high decomposition temperatures (T_d, corresponding to 5% weight loss) of 471 °C for **CDE1** and 507 °C for **CDE2** (Fig. S1†). Moreover, the glass transition temperatures (T_g) of these compounds reach up to 283 °C for **CDE1** and 289 °C for **CDE2** (Fig. S2†). To evaluate the morphological stability of these compounds, we utilized atomic force microscopy (AFM) to explore their surface images in neat films before and after annealing at 160 °C (Fig. S3†). Apparently, the surfaces of the neat films after annealing remained smooth and pinhole-free, almost the same as the unannealed surfaces. The good thermal and morphological stability of these materials guarantee homogeneous and stable amorphous thin films *via* solution processing, which is indispensable for the operation of OLEDs.

Fig. 2 shows the absorption, photoluminescence (PL) and phosphorescence spectra of **CDE1** and **CDE2** in film. Both compounds exhibit similar absorption profiles with two types of absorption bands: the absorption bands at 289 and 298 nm, which can be attributed to the π–π* transition of the carbazole dendrons;[11a] the charge-transfer (CT) absorption bands at 348 and 349 nm, which can be assigned to the π–π* electron transition from 9,9-dimethyl-9,10-dihydroacridine (DMAC) and the carbazole to the benzophenone. In their PL spectra in neat film, the emission peaks are blue-shifted with the increasing generation of the carbazole dendrons, indicating that the donor–acceptor feature of **CDE2** is weaker than that of **CDE1**, which can be verified by the TD-DFT calculation results (Fig. S6†).[11b,14] In comparison with the neat films, the toluene solutions of the two dendrimers exhibit bathochromic shifts of 31 and 33 nm, respectively (Fig. S4†). This implies that the intermolecular π–π* interactions of the fluorescent core in the solid state are significantly weakened by the bulky molecular structure of the external carbazole dendrons.[15] The energy gaps between the singlet and triplet state energy (ΔE_{ST}) are 0.11 eV for **CDE1** and 0.15 eV for **CDE2**, which were estimated from the onsets of the fluorescence and phosphorescence spectra. The small ΔE_{ST} values suggest that triplet excitons can be easily harvested by $T_1 \rightarrow S_1$ reverse intersystem crossing. The PLQYs of **CDE1** and **CDE2** in neat film were measured to be 0.77 and 0.75 under N_2 conditions, respectively, showing good potential in OLEDs.

To confirm the existence of the TADF in **CDE1** and **CDE2**, their transient PL spectra both in toluene and in neat film were measured. As shown in Fig. 3a and b, both compounds exhibit a second-order exponential decay in toluene under oxygen-free conditions with a delayed fluorescence (DF) decay of 523 ns (**CDE1**) and 627 ns (**CDE2**). Their prompt fluorescence decay lifetimes of 15 ns (**CDE1**) and 21 ns (**CDE2**) indicate the radiative decay from S_1 to S_0. After the exposure of the solution in

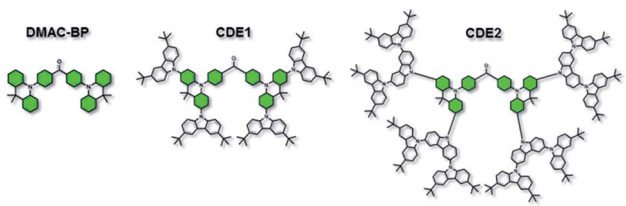

Fig. 1 Chemical structures of DMAC-BP, CDE1 and CDE2.

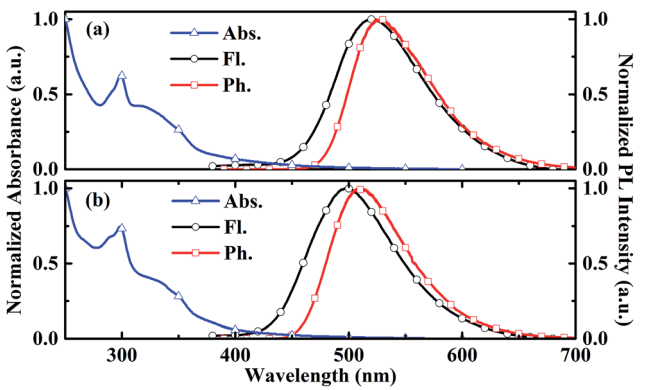

Fig. 2 The absorption and fluorescence spectra at room temperature, and phosphorescence spectra at 77 K of CDE1 (a) and CDE2 (b) in neat film.

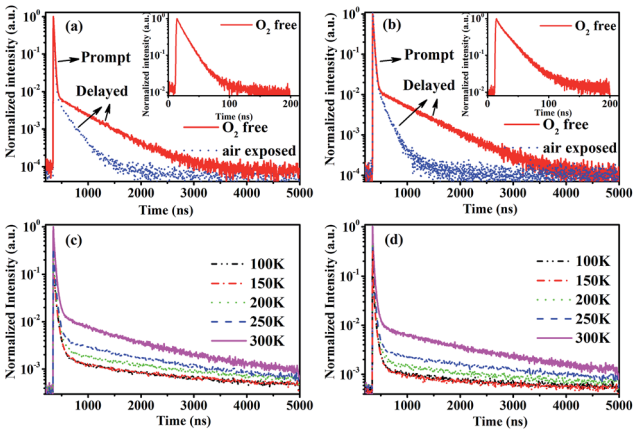

Fig. 3 Transient decay curves of **CDE1** (a) and **CDE2** (b) in toluene without and with oxygen exposure for 30 min. Inset: prompt fluorescence. Temperature dependence of the transient decay for **CDE1** (c) and **CDE2** (d).

ambient air for 30 minutes, the delayed component significantly decreases.[1b,16] This implies that PL decay is sensitive to oxygen, which proves that the two compounds feature typical TADF behavior. Moreover, the temperature-dependence of the transient PL decay in film is consistent with the typical characteristics of TADF materials. The delayed component gradually increases when raising the temperature from 100 to 300 K (Fig. 3c and d).[17]

Inspired by the highly thermal stability and good film forming ability of the two dendrimers, simple double-layer solution-processed OLEDs were fabricated with an architecture of ITO/PEDOT : PSS (30 nm)/**CDE1** (Devices A1–A4) or **CDE2** (Devices B1–B4) (70 nm)/TPBi (40 nm)/Liq (2 nm)/Al (Fig. 4), where poly(3,4-ethylenedioxythiophene) doped with poly(styrenesulfonate) (PEDOT : PSS) served as a hole-injecting layer and 1,3,5-tris(*N*-phenylbenzimidazol-2-yl)benzene (TPBi) acted as an electron transporting layer (ETL). Meanwhile, the EMLs were exposed to elevated temperatures at 80 (A2 and B2), 120 (A3 and B3) and 160 °C (A4 and B4), for comparison with those without thermal annealing (A1 and B1). The EML was spin-coated from chlorobenzene solution.

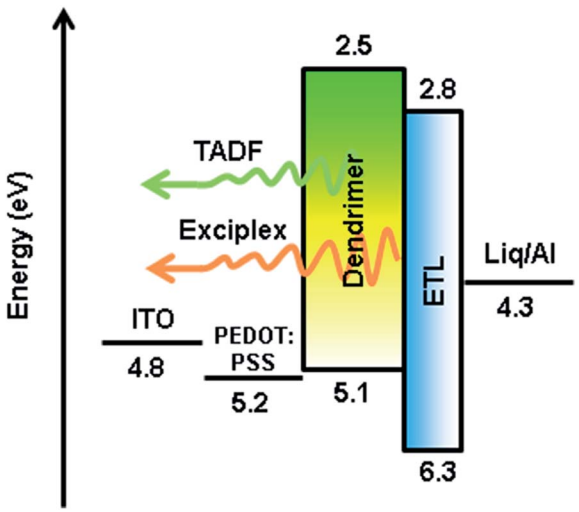

Fig. 4 Schematic diagram of the energy levels of Devices A1–B4.

Fig. 5 shows the EL spectra, the current density–voltage–luminance (*J*–*V*–*L*) characteristics, and the EQEs *versus* luminance curves of Devices A1–A4. The corresponding curves for Devices B1–B4 are shown in Fig. S8.† The characteristic data for all devices are summarized in Table 1. The driving voltages of Devices A1–A4 are significantly lower than the corresponding Devices B1–B4. For example, Device A2 exhibits driving voltage at 4.5 V that is lower than the 7.7 V of Device B2 at the same luminance of 10 cd m^{-2}. The superior electrical performance of **CDE1** is attributed to the better matched highest occupied molecular orbital (HOMO) and lowest unoccupied molecular orbital (LUMO) levels that lower the hole and electron injection barriers of Device A. Among Series A, Device A2 exhibits considerably high luminance and current density (Fig. 5a) at the same bias. A maximum current efficiency ($\eta_{c,max}$) of 38.9 cd A^{-1} (Fig. S7a†), a maximum power efficiency ($\eta_{p,max}$) of 17.3 lm W^{-1} (Fig. S7b†), and a maximum external quantum efficiency ($\eta_{ext,max}$) of 12.0% (Fig. 5b) were achieved. It is worth mentioning that these devices exhibit very high color stability at the elevated temperatures (see the inset of Fig. 5b) which is one of the prerequisites for practical application. Moreover, these devices show rather low efficiency roll-off values. At the luminance of 1000 cd m^{-2}, the η_{ext} of Device A2 is as high as 11.9%, and at the luminance of 5000 cd m^{-2}, the η_{ext} still remains at 10.3%.

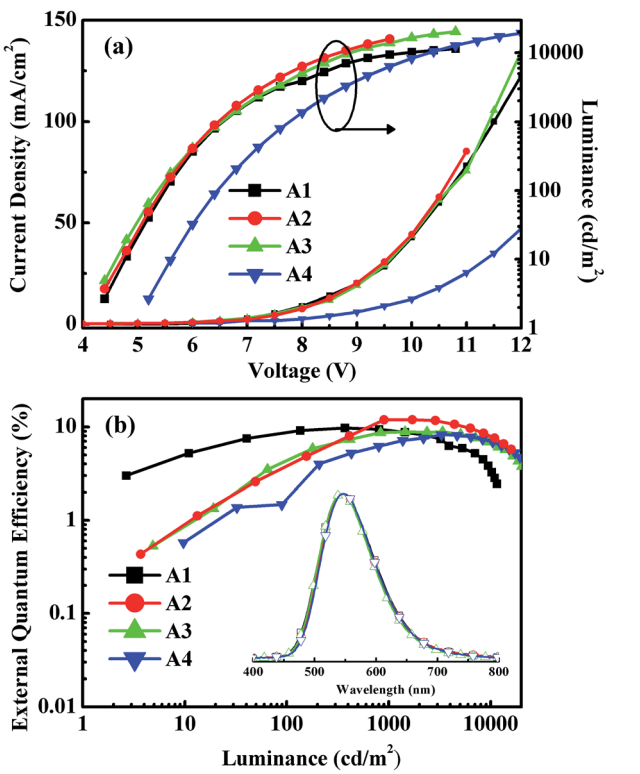

Fig. 5 (a) Current density–voltage–luminance (*J*–*V*–*L*) characteristics. (b) External quantum efficiency *versus* luminance curves of Devices A1–A4 and the EL spectra of **CDE1** annealed at different temperatures (inset).

Table 1 EL performances of the devices

Device	V_{10}[a] [V]	$\eta_{ext,max}$[b] [%]	$\eta_{ext,1000}$[c] [%]	L_{max} [cd m^{-2}]	λ_{ems}[d] [nm]	FWHM[e] [nm]	CIE(x, y)[f]
A1	4.9	9.7	9.0	>10 000	546	106	(0.38, 0.55)
A2	4.8	12.0	11.9	>10 000	546	103	(0.38, 0.56)
A3	4.7	8.8	8.7	>10 000	546	102	(0.38, 0.56)
A4	6.0	8.3	6.7	>10 000	546	101	(0.39, 0.55)
B1	9.4	3.3	2.0	1197	522	114	(0.32, 0.52)
B2	7.7	5.2	4.1	2512	522	118	(0.32, 0.51)
B3	8.1	5.2	4.1	2418	528	115	(0.32, 0.52)
B4	9.3	4.7	4.3	2278	528	112	(0.33, 0.53)
C3	4.4	13.8	13.3	>10 000	552	114	(0.40, 0.54)

[a] Voltage at 10 cd m^{-2}. [b] Maximum EQE. [c] EQE at 1000 cd m^{-2}. [d] Peak EL wavelength. [e] Full-width half maximum of the EL spectrum. [f] Commission Internationale de L'Eclairage (CIE) coordinates.

Interestingly, we find significant red-shifts (26 nm for **CDE1** and >23 nm for **CDE2**) of the EL spectra in comparison with their PL spectra (Table S1†). We suppose that the exciplex formed at the interface between the EML and the ETL contribute to the red-shift.[4a] To shed light on this hypothesis of exciplex existence, we fabricated devices based on **CDE1** with four different ETLs including 4,7-diphenyl-1,10-phenanthroline (BPhen) for Device C1, 4,6-Bis(3,5-di-3-pyridylphenyl)-2-methylpyrimidine (B3PYMPM) for Device C2, 1,3,5-tri[(3-pyridyl)-phen-3-yl]benzene (TmPyPB) for Device C3 and TPBi for Device C4. Apparently, all the devices with different ETLs exhibit red-shifts in the EL spectra (Fig. S11†) compared to the so-called single layer (without ETL) device (peak at 528 nm shown in Fig. S12†) with a full width at half maximum (FWHM) of 95 nm. Judging from Fig. S11 and 12,† it is evident that **CDE1** easily forms the interfacial exciplex with the ETLs through the external carbazole dendrons. Furthermore, we use a Gaussian function to fit the EL spectra curves and find that all of the EL spectra contain two main components which could be assigned to TADF emission (equivalent to that of Fig. S12†) and the exciplex emission which depends on the ETL (Fig. S13†).

Beyond the steady state study, to further prove the existence of the exciplex, we measured the transient decay of the mixtures of TmPyPB and **CDE1**. The steady state PL spectra of TmPyPB : **CDE1** films show gradual red-shifts on increasing the ratio of TmPyPB from 10 wt% to 50 wt% (Fig. 6a).[4a,18] Undoubtedly, the time-resolved PL spectroscopy data of the pristine **CDE1** film and the mixed TmPyPB : **CDE1** (1 : 1) film provide direct evidence of the existence of the exciplex. At the early delay stage (50 ns), the red-shift in the emission profile of the mixture is almost negligible compared to that of the neat film (Fig. 6b). In contrast, at the longer delayed time (at 1 μs), a distinguishable change is observed, which indicates that the exciplex contributes to red-shift of the spectra. The red-shifted delayed emission is quite similar to the spectral fitting (Fig. S13c†) of the device with TmPyPB as the ETL.[4b,19] All of the aforementioned evidence sufficiently proves the existence of the two parallel emission mechanisms: intrinsic TADF from the dendrimer and the exciplex emission at the interface between the EML and the ETL. Among Device Series C, the Device C3 with TmPyPB as the ETL achieves a maximum EQE of up to 13.8% (Fig. S10b†), partially due to the high electron mobility and excellent hole blocking ability of TmPyPB. Table 2 summarizes the performances of the state-of-the-art OLEDs with TADF or exciplex emission reported in recent literature. It can be seen that very few emitters achieved high efficiencies at 5000 cd m^{-2}. Basically, regardless of wet or dry processes, only the host-guest structure could maintain high efficiencies at high luminance. In contrast, the dendrimer-based non-doped

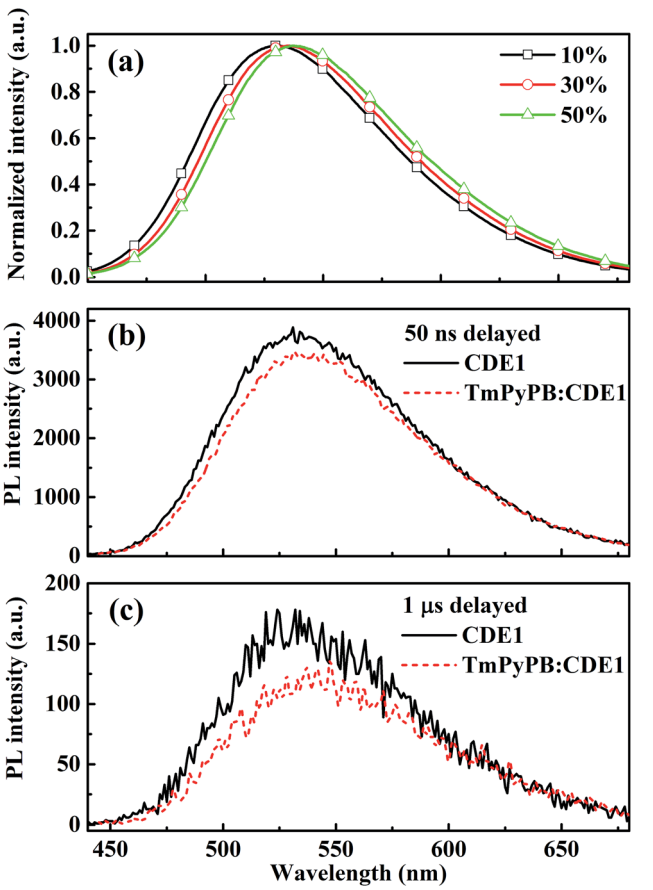

Fig. 6 (a) Steady state PL spectra of **CDE1** doped with 10, 30 and 50 wt% TmPyPB in film. Time-resolved transient fluorescence spectra delayed at 50 ns (b) and 1 μs (c) for **CDE1** and TmPyPB : **CDE1** (1 : 1) in film, respectively.

Table 2 Comparison of highly efficient OLEDs with TADF or exciplex emission

	Process	Architecture	EML	Mechanism	$\eta_{ext,max}$ [%][a]	$\eta_{ext,1000}$ [%][b]	$\eta_{ext,5000}$ [%][c]	Roll-off [%][d]
This work	Sol[e]	Double[f]	Non-doped	TADF and exciplex	12.0[g]	11.9	10.3	13.4
					13.8[h]	13.3	8.2	38.3
Ref. 6a	Sol	Double	Non-doped	TADF	3.4	1.5	—[i]	—
Ref. 9	Sol	Double	Doped	TADF	15.2	13.3	8.8	33.8
Ref. 6b	Sol	Double	Doped	TADF	11.3	10.6	6.9	34.9
Ref. 8	Sol	Four	Doped	TADF	18.3	12.0	6.0	50
Ref. 7a	Sol	Double	Doped	TADF	18.6	13.0	8.0	38.5
Ref. 20	Sol	Double	Doped	TADF	5.2	3.0	—	—
Ref. 12	Vac[j]	Double	Non-doped	TADF	10.6	10.6	10.2	3.8
Ref. 5	Vac	Three	Doped	Exciplex	15.4	8.6	—	—
Ref. 18	Vac	Four	Doped	Exciplex	>14	6.5	—	—
Ref. 4a	Vac	Double	Doped	Exciplex	12.2	6.0	—	—

[a] Maximum EQE. [b] EQE at 1000 cd m^{-2}. [c] Measured at 1000 cd m^{-2}. [d] The roll-off of the EQE from 1000 to 5000 cd m^{-2}. [e] Solution-processed device. [f] Double-layer device. [g] Device C4 with TBPi as the ETL. [h] Device C3 with TmPyPB as the ETL. [i] Not available. [j] Vacuum evaporated device.

double-layer architectures boost the EQE to 11.9% (TPBi as the ETL) and 13.3% (TmPyPB as the ETL) at a luminance of 1000 cd m^{-2}. Impressively, the roll-offs of the EQEs from 1000 to 5000 cd m^{-2} are reasonably low compared to those of the counterpart devices, which could be ascribed to the self-host like nature of the dendrimer based emitters. To the best of our knowledge, the peak EQE and the luminance of **CDE1** are some of the highest among the non-doped dendrimer-based OLEDs featuring a TADF mechanism.

Conclusions

In conclusion, we have developed two new carbazole-dendronized emitters based on a green emissive TADF core. Both dendrimers possess excellent thermal stability, good solution processability, and an obvious TADF feature accompanied by hidden exciplex emission. A non-doped OLED based on the dendrimer of **CDE1** formed by a solution process exhibits a high EQE of 13.8% compared to recent simple dendrimer-based OLEDs, which is contributed to by two parallel emissive channels of TADF and exciplex emission fully harvesting all the generated excitons. This work presents a judicious design strategy for non-doped solution-processable TADF emitters, and reveals a new emissive approach by combining both TADF and exciplex emission. We believe that the strategy will pave the way to practical application of solution-processable fluorescent OLEDs for displays and lighting sources.

Experimental section

General information

All reagents were purchased from commercial sources and used as received without further purification. Solvents for synthesis were purified according to standard procedures prior to use. ^{1}H NMR and ^{13}C NMR spectra were measured on a MERCURYVX300 or Bruker Advanced II (400 MHz) spectrometer. Elemental analysis of carbon, hydrogen, and nitrogen was obtained using a Vario EL III microanalyzer. MALDI-TOF (matrix-assisted laser-desorption/ionization time-of-flight) mass spectra were performed on a Bruker BIFLEX III TOF mass spectrometer. UV-vis absorption spectra were collected on a Shimadzu UV-2700 recording spectrophotometer. Photoluminescence (PL) spectra were collected on a Hitachi F-4600 fluorescence spectrophotometer. Absolute PLQYs were measured on a Quantaurus-QY measurement system (C11347-11, Hamamatsu Photonics) and all the samples were excited at 330 nm. Thermogravimetric analysis (TGA) was undertaken with a NEZSCH STA 449C instrument and the thermal stability of the samples under nitrogen flow was investigated at a heating rate of 15 °C min^{-1} from 25 °C to 800 °C. Differential scanning calorimetry (DSC) was performed using a NETZSCH DSC 200 PC unit at a heating rate of 10 °C min^{-1} from room temperature to 300 °C under a nitrogen flow. Cyclic voltammetry (CV) was measured on a CHI voltammetric analyzer with the conventional three-electrode configuration which consists of a platinum working electrode, a platinum wire auxiliary electrode, and an Ag wire pseudo reference electrode with ferrocenium-ferrocene (Fc^+/Fc) as the internal standard. Tetrabutylammonium hexaflorophosphate ($TBAPF_6$) (0.1 M) was used as the supporting electrolyte. Cyclic voltammograms were obtained at a scan rate of 100 mV s^{-1}. The onset potential was determined from the intersection of two tangents drawn at the rising and background current of the cyclic voltammogram.

Device fabrication and characterizations

Patterned indium tin oxide (ITO) coated glass substrates with a sheet resistance of 15–20 ohm/square underwent a wet-cleaning course in an ultrasonic bath, beginning with acetone, followed by ethanol. After UV-Ozone treatment for 20 min, a 30 nm thick PEDOT : PSS layer used as a hole-injecting layer was spin-coated on the ITO substrate and then baked inside the glove-box at 120 °C for 10 min. The EML was prepared by spin-coating from chlorobenzene solution on top of the PEDOT : PSS layer. The electron-transporting material was thermally evaporated onto the emitter layer in a vacuum chamber. Finally, Al was sequentially deposited through a shadow mask successively to define the size of the active area. Except for the spin-coating of the PEDOT : PSS layer, all the solution processes were carried

out in the controlled atmosphere of a nitrogen dry-box containing less than 0.1 ppm oxygen and moisture. The devices were encapsulated with UV-curable epoxy before being taken out from the glove-box. All the measurements were carried out at room temperature under ambient conditions.

Synthesis

The solvents (1,4-dioxane, and chloroform) were purified by a conventional procedure and distilled under dry argon before using.

Bis(4-(2,7-diiodo-9,9-dimethylacridin-10(9*H*)-yl)phenyl) methanone (4IDMACBP). A mixture of bis(4-(9,9-dimethylacridin-10(9*H*)-yl)phenyl)methanone (2.38 g, 4 mmol), *N*-iodosuccinimide (3.60 g, 16 mmol) and $CHCl_3$ (100 mL) was stirred at 50 °C in the absence of light for 96 hours. After cooling, the reaction was quenched with a saturated aqueous solution of $Na_2S_2O_3$, the reaction mixture was extracted with dichloromethane, and dried with anhydrous Na_2SO_4. After removal of the solvent, the residue was purified by column chromatography on silica gel using dichloromethane/petroleum ether (3 : 2 by vol.) as the eluent to give a green powder. Yield 92%. ^{1}H NMR ($CDCl_3$, 400 MHz): δ [ppm] 1.66 (s, 12H), 6.08 (d, J = 8.8 Hz, 4H), 7.29 (d, J = 8.8 Hz, 4H), 7.49 (d, J = 8.4 Hz, 4H), 7.71 (s, 4H), 8.18 (d, J = 8.4 Hz, 4H). ^{13}C NMR ($CDCl_3$, 100 MHz): δ [ppm] 194.5, 144.5, 139.8, 137.1, 135.3, 134.1, 132.9, 132.6, 131.0, 116.4, 83.9, 36.0, 31.0. MALDI-TOF (m/z): 1085.0 [$M^+ - CH_3$]. Anal. calcd for $C_{43}H_{32}I_4N_2O$ (%): C, 46.94; H, 2.93; N, 2.55; O, 1.45. Found: C, 46.72; H, 3.02; N, 2.63.

Bis(4-(2,7-bis(3,6-di-*tert*-butyl-9*H*-carbazol-9-yl)-9,9-dimethylacridin-10(9*H*)-yl)phenyl)methanone (CDE1). A mixture of 3,6-di-*tert*-butyl-9*H*-carbazole (0.59 g, 2 mmol), 4IDMACBP (1.10 g, 1 mmol), CuI (3.80 mg, 0.02 mmol), K_3PO_4 (4.24 g, 20 mmol), (±)-*trans*-1,2-cyclohexanediamine (3.42 mg, 0.03 mmol) and 1,4-dioxane (8 mL) was heated at 110 °C under argon for 48 h. After cooling, the reaction mixture was diluted with brine, extracted with dichloromethane, and dried with anhydrous Na_2SO_4. After removal of the solvent, the residue was purified by column chromatography on silica gel using dichloromethane/petroleum ether (1 : 1 by vol.) as the eluent to give a green powder. Yield 73%. ^{1}H NMR ($CDCl_3$, 400 MHz): δ [ppm] 1.36 (s, 72H), 1.74 (s, 12H), 6.53 (d, J = 8.8 Hz, 4H), 7.24 (d, J = 8.8 Hz, 4H), 7.28 (dd, J = 8.8, 2.0 Hz, 8H), 7.42 (dd, J = 8.4, 2.0 Hz, 8H), 7.70 (d, J = 2.0 Hz, 4H), 7.87 (d, J = 8.4 Hz, 4H), 8.23 (d, J = 1.6 Hz, 8H), 8.26 (d, J = 8.4 Hz, 4H). ^{13}C NMR ($CDCl_3$, 100 MHz): δ [ppm] 194.7, 145.2, 142.5, 139.5, 139.1, 137.2, 133.0, 131.5, 131.4, 131.3, 125.2, 124.4, 123.5, 123.1, 116.3, 115.2, 109.4, 36.6, 34.7, 32.0, 31.6. MALDI-TOF (m/z): 1690.7 [$M^+ - CH_3$]. Anal. calcd for $C_{123}H_{128}N_6O$ (%): C, 86.58; H, 7.56; N, 4.93; O, 1.45. Found: C, 86.43; H, 7.66; N, 4.88.

Bis(4-(2,7-bis(3,3″,6,6″-tetra-*tert*-butyl-9′*H*-[9,3′:6′,9″-tercarbazole]-9′-yl)-9,9-dimethylacridin-10(9*H*)-yl)phenyl)methanone (CDE2). Prepared according to the same procedure as used for **CDE1** but using 3,3″,6,6″-tetra-*tert*-butyl-9′*H*-9,3′,6′,9″-tercarbazole. Yield 65%. ^{1}H NMR ($CDCl_3$, 400 MHz): δ [ppm] 1.46 (s, 144H), 1.98 (s, 12H), 6.76 (d, 8.8 Hz, 4H), 7.34 (d, 8.8 Hz, 16H), 7.47–7.45 (m, 20H), 7.65–7.60 (m, 16H), 7.87 (d, J = 8.0 Hz, 4H), 7.91 (s, 4H), 8.16 (s, 16H), 8.26 (s, 8H), 8.44 (d, J = 8.0 Hz, 4H). ^{13}C NMR ($CDCl_3$, 100 MHz): δ [ppm] 194.5, 145.0, 142.5, 140.7, 140.1, 139.9, 137.5, 133.3, 131.6, 130.8, 130.7, 126.0, 125.7, 124.8, 123.7, 123.5, 123.1, 119.4, 116.2, 115.6, 111.0, 109.0, 36.9, 34.7, 32.0, 31.7. MALDI-TOF (m/z): 3459.0 [$M^+ - CH_3$]. Anal. calcd for $C_{251}H_{248}N_{14}O$ (%): C, 86.71; H, 7.19; N, 5.64; O, 0.46. Found: C, 86.65; H, 7.41; N, 5.52.

Acknowledgements

We gratefully acknowledge financial support from the National Basic Research Program of China (973 Programs 2015CB655002 and 2013CB834805), the National Natural Science Foundation of China (Nos. 91433201, 61575146, 51573141 and 51125013), the Innovative Research Group of Hubei Province (No. 2015CFA014) and the Fundamental Research Funds for the Central Universities of China.

Notes and references

1 (*a*) K. Goushi, K. Yoshida, K. Sato and C. Adachi, *Nat. Photonics*, 2012, **6**, 253; (*b*) H. Uoyama, K. Goushi, K. Shizu, H. Nomura and C. Adachi, *Nature*, 2012, **492**, 234.

2 (*a*) Q. Zhang, B. Li, S. Huang, H. Nomura, H. Tanaka and C. Adachi, *Nat. Photonics*, 2014, **8**, 326; (*b*) S. Hirata, Y. Sakai, K. Masui, H. Tanaka, S. Y. Lee, H. Nomura, N. Nakamura, M. Yasumatsu, H. Nakanotani, Q. Zhang, K. Shizu, H. Miyazaki and C. Adachi, *Nat. Mater.*, 2015, **14**, 330.

3 B. S. Kim and J. Y. Lee, *Adv. Funct. Mater.*, 2014, **24**, 3970.

4 (*a*) D. Chen, G. Xie, X. Cai, M. Liu, Y. Cao and S. Su, *Adv. Mater.*, 2016, **28**, 239; (*b*) D. Graves, V. Jankus, F. B. Dias and A. P. Monkman, *Adv. Funct. Mater.*, 2014, **24**, 2343.

5 X. Liu, Z. Chen, C. Zheng, C. Liu, C. S. Lee, F. Li, X. Ou and X. Zhang, *Adv. Mater.*, 2015, **27**, 2378.

6 (*a*) K. Albrecht, K. Matsuoka, K. Fujita and K. Yamamoto, *Angew. Chem., Int. Ed.*, 2015, **54**, 5677; (*b*) C. Tang, T. Yang, X. Cao, Y. Tao, F. Wang, C. Zhong, Y. Qian, X. Zhang and W. Huang, *Adv. Opt. Mater.*, 2015, **3**, 786.

7 (*a*) Y. Wada, K. Shizu, S. Kubo, K. Suzuki, H. Tanaka, C. Adachi and H. Kaji, *Appl. Phys. Lett.*, 2015, **107**, 183303; (*b*) C. Liu, Y. Li, Y. Li, C. Yang, H. Wu, J. Qin and Y. Cao, *Chem. Mater.*, 2013, **25**, 3320.

8 Y. J. Cho, K. S. Yook and J. Y. Lee, *Adv. Mater.*, 2014, **26**, 6642.

9 G. Xie, X. Li, D. Chen, Z. Wang, X. Cai, D. Chen, Y. Li, K. Liu, Y. Cao and S. Su, *Adv. Mater.*, 2016, **28**, 181.

10 (*a*) J. Ding, B. Wang, Z. Yue, B. Yao, Z. Xie, Y. Cheng, L. Wang, X. Jing and F. Wang, *Angew. Chem., Int. Ed.*, 2009, **48**, 6664; (*b*) X. Wang, S. Wang, Z. Ma, J. Ding, L. Wang, X. Jing and F. Wang, *Adv. Funct. Mater.*, 2014, **24**, 3413.

11 (*a*) D. Xia, B. Wang, B. Chen, S. Wang, B. Zhang, J. Ding, L. Wang, X. Jing and F. Wang, *Angew. Chem., Int. Ed.*, 2014, **53**, 1048; (*b*) J. Ding, J. Lu, Y. Cheng, Z. Xie, L. Wang, X. Jing and F. Wang, *Adv. Funct. Mater.*, 2008, **18**, 2754.

12 Q. Zhang, D. Tsang, H. Kuwabara, Y. Hatae, B. Li, T. Takahashi, S. Y. Lee, T. Yasuda and C. Adachi, *Adv. Mater.*, 2015, **27**, 2096.

13 F. Schlutter, F. Rossel, M. Kivala, V. Enkelmann, J. P. Gisselbrecht, P. Ruffieux, R. Fasel and K. Mullen, *J. Am. Chem. Soc.*, 2013, **135**, 4550.
14 T. Qin, J. Ding, L. Wang, M. Baumgarten, G. Zhou and K. Mullen, *J. Am. Chem. Soc.*, 2009, **131**, 14329.
15 (*a*) P. Moonsin, N. Prachumrak, S. Namuangruk, S. Jungsuttiwong, T. Keawin, T. Sudyoadsuk and V. Promarak, *Chem. Commun.*, 2013, **49**, 6388; (*b*) N. Prachumrak, S. Pojanasopa, S. Namuangruk, T. Kaewin, S. Jungsuttiwong, T. Sudyoadsuk and V. Promarak, *ACS Appl. Mater. Interfaces*, 2013, **5**, 8694.
16 (*a*) Q. Zhang, J. Li, K. Shizu, S. Huang, S. Hirata, H. Miyazaki and C. Adachi, *J. Am. Chem. Soc.*, 2012, **134**, 14706; (*b*) H. Kaji, H. Suzuki, T. Fukushima, K. Shizu, K. Suzuki, S. Kubo, T. Komino, H. Oiwa, F. Suzuki, A. Wakamiya, Y. Murata and C. Adachi, *Nat. Commun.*, 2015, **6**, 8476.
17 H. Wang, L. Xie, Q. Peng, L. Meng, Y. Wang, Y. Yi and P. Wang, *Adv. Mater.*, 2014, **26**, 5198.
18 V. Jankus, P. Data, D. Graves, C. McGuinness, J. Santos, M. Bryce, F. B. Dias and A. P. Monkman, *Adv. Funct. Mater.*, 2014, **24**, 6178.
19 G. Mallesham, C. Swetha, S. Niveditha, M. E. Mohanty, N. J. Babu, A. Kumar, K. Bhanuprakash and V. Rao, *J. Mater. Chem. C*, 2015, **3**, 1208.
20 L. Mei, J. Hu, X. Cao, F. Wang, C. Zheng, Y. Tao, X. Zhang and W. Huang, *Chem. Commun.*, 2015, **51**, 13024.